Spent coffee ground as a renewable source of energy: analysis of bulk powder flowability

L. M. Sousa[1] and M. C. Ferreira[1*]

[1]Drying Center for Pastes, Suspensions, and Seeds, Chemical Engineering Department, Federal University of São Carlos, P.O. Box 676, 13565-905 São Carlos, Brazil

ABSTRACT

The main use for Spent Coffee Ground (SCG) produced in the soluble coffee industry is the thermal energy generation in the industry itself. Throughout processing, SCG is submitted to unit operations strongly dependent on the powder flow behavior. In this study, we evaluated two classical flowability indexes of non-consolidated SCG powder: the angle of repose (AoR) and the Hausner ratio (HR). The influence of the mean diameter, particle size distribution and moisture content on AoR and HR of SCG was analyzed for powders with particle mean sizes from 225 to 550 μm. Values of HR>1.35 and AoR>45°, which characterize a poor flowability, were observed for powders of mean particle size close to 350 μm and for mixtures with more than 40% of fine particles in their composition. The AoR was sensitive to powder size distribution, and powders with similar mean sizes presented higher values of AoR when the mixture size span was larger. For powders with moisture content up to 50%, the flowability indexes were not significantly affected by the moisture content. The Linear Mixture-Packing Model was used to predict the packed-bed void fraction for binary and ternary mixtures made up from the combination of three base powders of different sizes.

* Corresponding author. Tel.: +55 16 33518442. E-mail address: mariaf@ufscar.br (M. C. Ferreira).
Abbreviations: AoR-angle of repose; HR-Hausner ratio; PSD-particle size distribution; SCG-spent coffee ground; SCI-soluble coffee industry.

The model was used to build up a ternary diagram that is able to estimate HR of the powder mixtures. Additionally, an equation was fitted to correlate HR and AoR. The proposed diagram and the fitted equation may provide insight into the flow behavior and help process design of industrial plants that handle SCG.

*Keywords: s*pent coffee ground; biomass, flowability; Hausner ratio; Angle of Repose.

1. Introduction

In 2016, more than 9 million tons of coffee beans were produced worldwide (International Coffee Organization, 2017), generating a revenue around US$ 25 billion (Brazilian Coffee Exporters Council, 2017). In emerging countries well-known as traditional coffee producers, such as Brazil, Colombia and Vietnam, coffee is a commodity that plays a major contribution in the trade market. Fruit and beans are processed to produce the coffee powder, which is further sent to the Soluble Coffee Industry (SCI) or directly for domestic brewing. These processes generate a huge amount of solid residue, the Spent Coffee Ground (SCG). Around 2.5 million tons of SCG were produced in 2016, which was readily available for industrial processing (Instant Coffee Market, 2017; Mussatto, Machado, Martins, & Teixeira, 2011). If disposed of in landfills without a previous treatment, this residue might cause serious environmental issues due to its high organic load and acidity (Mussatto et al., 2011). The high calorific power of SCG (close to 25 kJ/kg, which is similar to that of the coal) (Silva, Nebra, Machado Silva, & Sanchez, 1998), makes it an attractive biomass for thermal energy generation in SCI facilities. Applications involving the production of biodiesel (Al-Hamamre, Foerster, Hartmann, Kröger, & Kaltschmitt, 2012; Kondamudi, Mohapatra, & Misra, 2008; Liu, Tu, Knothe, & Lu, 2017), fuel pellets (Kondamudi et al., 2008; P. Li, Kanda, & Makino, 2014), hydrogen and ethanol (Mussatto et al., 2011) have been reported for this solid waste but most of it is burned in SCI furnaces for steam production. Almost the

total energy required in SCI is supplied by SCG (Silva et al., 1998), thus significantly reducing the soluble coffee cost production. An effective handling of biomass powders through the related unit operations is of key importance to the success of those thermochemical processes.

In spite of the attractive energy balance, some critical issues can arise in handling biomass powders, such as the blockage of pipes, feeding devices or silos outlets (Dai, Cui, & Grace, 2012). Such occurrences may prevent a continuous and uniform flow to furnaces, reactors and so on, thus disrupting operations and reducing the overall efficiency and productivity. The effectiveness of feeding, storage, compaction and transport operations is strongly dependent on the powder flow behavior. The ability of a powder to flow is ruled by complex interactions between attractive and external field forces. If the weight of the particles is much larger than the attractive interparticle forces they will flow well, otherwise, a cohesive behavior is expected. Interparticle adhesion is originated by intermolecular forces including van der Waals forces, local chemical bonds, electrostatic charges, and bridging forces originated by liquid surface tension (Li, Rudolph, Weigl, & Earl, 2004). Van der Waals forces of molecular origin are dominant in fine dry powders and the bridging forces become significant as the water saturation in moist bulk powders increases (Althaus & Windhab, 2012; Castellanos, 2005). The numerous mechanisms that play a role in powder flowability have not been fully understood yet and quantifying flowability is quite a challenging task. However, it is known to depend on a number of factors including the particle size, size distribution, shape, surface texture, surface energy, chemical composition, moisture content, vessel geometry, packing history, among others (Li et al., 2004).

The Hausner ratio (HR) and the Angle of Repose (AoR) are indexes based on easily measurable properties that serve as useful flowability indicators for bulk powders in industrial and practical applications. The first one is based on the ratio of tapped to loose bulk density

and is considered a measure of powder cohesion, while the latter is obtained from powder flow under gravitational discharge (Abdullah & Geldart, 1999). As particle size distribution and moisture content of SCG produced in SCIs can vary in a wide range (Silva et al., 1998), assessing how SCG flowability is affected by these variables is useful for monitoring process operations and quality features. Although the composition and energetic characteristics of SCG have been widely investigated in the literature (Ballesteros, Teixeira, & Mussatto, 2014; Campos-Vega, Loarca-Piña, Vergara-Castañeda, & Oomah, 2015; Mussatto et al., 2011; Silva et al., 1998), to the best of authors' knowledge, no study was focused on assessing their basic flowability characteristics.

This study is aimed at evaluating flow indexes of non-consolidated SCG powders. The AoR and HR were determined for dry and moist powders in a size range from 225 to 550 μm and the influence of mean size and moisture content on the flowability indexes was evaluated. To be able to cover a wide range of particle's size and particle size distribution, three SCG powder samples made of fine, intermediary and coarse size particles were used to produce binary and ternary mixtures. A ternary diagram was built up to predict HR of SCG powder mixtures based on the Modified-Linear Mixture Packing model and an equation correlating HR and AoR was fitted based on the experimental data.

2. Material and Methods

The procedures used for sample preparation, particle and bulk powder characterization and measurement of flow indexes will be presented in this section.

2.1 Sample preparation

The SCG was obtained after brewing an ordinary Brazilian ground coffee made up from a blend of Arabica and Robusta grains (brand Três Corações), acquired in São Carlos-SP,

Brazil. To reduce the powder's moisture content, 5 mm thick layer samples were oven-dried at 105±2ºC for 24h and stored under ambient temperature until further use.

The particle size analysis of the original dried sample was performed by sieving it according to the ASTM standards (ASTM International, 2010), in triplicate assays. SCGs samples of 100 g were poured into a set of stainless steel sieves, with size apertures decreasing from 2360 to 63 µm. The set of sieves was coupled to a shaker (RETSCH AS200) and vibrated during 30 min at an amplitude of 1.5 mm. The powder mass fraction retained in the sieves of size aperture above 600 µm, which was only 20% of the total, was discarded and the remaining portion was sieved again from 600 to 150 µm. This portion was separated into three fractions denominated as the base samples, A, B and C. Sample A is made up of particles with sizes between 600 and 500 µm (d_{svA}=550 µm), sample B contains the particles retained between 500 and 300 µm (d_{svB}=400 µm), and sample C those retained between 300 and 150 µm (d_{svC}=225 µm). Additional mixtures were produced by combining mass fractions (y) of 20, 40, 60 and 80% of the base samples, resulting in 12 binary and 6 ternary mixtures. The mixtures were homogenized prior to the assays. Tests were carried out in triplicate for the base powders, binary and ternary mixtures, therefore 63 dry samples were prepared and analyzed.

2.2 Powder characterization

The samples were characterized according to the methods described in the following sections.

2.2.1 Mean diameter

The mean diameter of the base samples, binary and ternary mixtures were calculated from Eq. (1), in which y_i is the mass fraction of the base sample (A, B or C) in the mixture and d_{svi} is the sieve mean diameter of the base sample.

$$d_S = 1/\sum(y_i/d_{svi}) \quad (1)$$

2.2.2 Initial moisture content

The initial moisture content was determined by the gravimetric method, in triplicate. Powder samples of 3 g were kept in an oven (FANEM, model 315SE) at 105 ºC for 24 h.

2.2.3 Solid and particle densities

The solid density (ρ_s) was determined for the SCG original dry sample using a helium gas pycnometer (Ultrapycnometer 1000, Quantachrome Instruments), in triplicate. The particle density (ρ_p) was determined for the dry base powders A, B and C using a liquid pycnometer, with a replicate. The pycnometer has a volume of 25 cm^3 and the liquid used was methanol.

2.2.4 Particle morphology

Particles shape and surface texture were evaluated through a scanning electron microscope (SEM). The SCG base samples were glued over a carbon tape and coated with gold. The analysis was performed using a microscope (FEI Inspect S50) under a high vacuum atmosphere.

2.2.4 Loose and tapped bulk densities

The loose and tapped bulk densities were obtained according to the procedure described elsewhere (Organization, 2012), in triplicate. Powder samples (50-70g) were poured through a funnel into a 250 cm^3 and 2.2 cm diameter graduated glass cylinder. In all the assays, the powder filled more than 60% of the cylinder volume. The vessel was placed into a proper tapping device that allowed the vessel to be successively lifted at a height of 3 cm and released (Campos & Ferreira, 2013). The powder volume was periodically recorded from N=0 up to N=1250 taps, when no more variation in the powder volume was observed. The assays were performed at ambient temperature and relative humidity between 45 and 70%, which is sufficient to eliminate static charges. Both the loose (initial) and tapped (final) bulk densities were obtained by dividing the powder mass in the cylinder by its respective volume. The loose or tapped void fractions were determined according to:

$$\varepsilon = 1 - \left(\rho_b^* / \rho_p\right) \tag{2}$$

where ρ_b^* is the loose (ρ_{lb}) or tapped (ρ_{tb}) bulk densities and ρ_p is the particle density. It is worth noting that Eq. (2) applies to estimate the void fractions of dry samples.

2.2.6 Powder humidification

To vary the powder moisture content, a humidification procedure was performed. A powder sample of 50 g was mixed with water in glass flasks, which were sealed and stored at 4°C for 60 h. After every 24 h, the flasks were opened and the powders were homogenized to ensure uniform moisture distribution.

The water amount added to the flasks were determined based on the established moisture content for a sample and covered a range of moisture content up to 50% (wet basis). For each base sample, four different moisture contents were analyzed in triplicate, therefore a

set of 36 moist samples was prepared. The moisture content in wet basis and the water saturation stage (S) in the bulk powders were calculated by:

$$MC = m_w/(m_w + m_s) \quad (3)$$

$$S\ (\%) = V_w/(V_t - V_s) \quad (4)$$

where m_w is the mass of liquid water in the packed-bed, m_s is the mass of solids, V_w is the total volume of liquid water in the packed-bed; V_t is the total volume of the compacted dry bed, and V_s is the volume occupied by the solids (based on ρ_s).

2.3 Flowability indicators

The powder flowability was assessed through measurements of AoR and HR, as described in the following sections. The criteria for flowability classification based on these indexes are described in details elsewhere (Tan, Morton, & Larson, 2015). According to these criteria, the transition from a *passable* to a *poor* flowability, which defines the likely limit to flow issues occurs for AoR and HR higher than 45° and 1.35, respectively.

2.3.1 Hausner ratio (HR)

HR was calculated from the ratio of the tapped to the loose bulk density, according to:

$$HR = \rho_{tb}/\rho_{lb} \quad (5)$$

2.3.2 Angle of Repose (AoR)

The angle of repose was determined by the funnel method, according to (ASTM International, 2000). The powders were poured into the funnel and discharged by gravity over a white paper surface, forming a conical heap of height H. The conical bed circumference was

drawn with a pen and its diameter (D) was taken as the average of four records. The experiments were performed in triplicate and AoR was calculated by:

$$AoR = \tan^{-1}(2H/(D-d)) \quad (6)$$

2.4 Statistical analysis

The one-way analysis of variance (ANOVA) based on the Tukey test was used to verify whether there was any statistically significant difference ($p<0.05$) between the means of the different groups of bulk densities and flow properties. The data are reported as mean values and their standard deviations.

The empirical equations fitted to the experimental data using the Excel software (Microsoft) and the determination coefficients for the equations (R^2) are reported.

3. Results and Discussion

The results for powder characterization and measurement of flowability indexes are presented in the following sections.

3.1 Characterization of SCG base dry samples

The main physical properties of the base samples are summarized in Table 1. The particle densities (ρ_p) of the base samples are similar to the value reported by Silva et al. (1998) for SCGs (1200 kg/m³) (Silva et al., 1998). The solid density is equal to 1315±3 kg/m³, which is similar to values reported for fresh coffee powders from Colombia and Mexico (respectively 1361 and 1355 kg/m³) (Singh, Singh, Bhamidipati, Singh, & Barone, 1997). Based on their mean size and particle density, the base powders A and B are classified as *Geldart B* and powder C is classified as *Geldart A* (Geldart, 1973). According to this

classification, samples A and B are coarse powders and sample C is categorized as a fine powder, but not a cohesive type.

(Table 1)

The loose bulk densities of powders A and B are higher than those of sawdust, rice straw (Guo, Chen, Xu, & Liu, 2015), sugarcane bagasse and corn stover (Dhiman et al., 2016). Due to the high combustion heat value of SCG powders, this is an appealing result concerning economic feasibility of using SCG as a fuel feedstock, as the costs for storage and transport would be lower and its energy density (in MJ/m^3) higher in comparison to those biomasses. After drying, the maximum moisture content of the base samples is equal to 5.4% (w.b.), and the saturation level (S) is less than 4%, characteristic of a pendular state in which discrete liquid bridges bind the particles together (Althaus & Windhab, 2012). Therefore, the contribution of the capillary forces is negligible to powder cohesion in the conditions tested.

The particle morphology and surface of powders A, B and C can be observed in Fig. 1.

(Fig. 1)

In all samples one can notice particles with quite irregular shapes and rough surfaces, with asperities on them, characteristics which are similar to those reported in the literature for SCG powders (Ballesteros et al., 2014; Zarrinbakhsh, Wang, Rodriguez-Uribe, Misra, & Mohanty, 2016).

3.2 Effect of d_S and particle size distribution on the flowability indexes

The measured values of HR are presented in Fig. 2 as a function of the mean diameter.

(Fig. 2)

The literature reports that flow indexes may be poorly reproducible because it is difficult to eliminate the past history of powders and to reproduce a macroscopically equivalent initial state in all the experiments (Castellanos, 2005). In the present study, the

standard deviations of HR (triplicate measurements) were in general lower than 5%, corroborating that the experimental procedures were effective to reduce variability.

In Fig. 2, the results for the base powders A, B and C are indicated by hollow circles, while the binary (AB, BC, and AC) and ternary mixtures (ABC) are indicated by solid symbols and hollow squares, respectively. The mixtures were obtained by combining the base powders, as described in Section 2.1, therefore some powders have similar mean sizes but different particle size distribution (PSD).

According to Fig. 2, the coarse powders A and B have similar HR (1.21±0.03 and 1.21±0.05, respectively) and both are categorized as *free-flowing* materials. As for sample C, which is the fine powder, HR increases to 1.50±0.03, which characterizes a *very poor* flowability. The transition from a *passable* to a *poor* flowability (HR>1.35) is observed at a particle size of 350 μm. Some authors (Li et al., 2004) observed that HR can be a misleading flowability indicator for particles having high adhesiveness, or a very broad size distribution and irregular shapes and in tests with pharmaceutical powders they found discrepancies between the HR results in comparison to real flow situations. However, the cohesive behavior of powder C was clearly noticeable during the experiments and is corroborated by the AoR results, as will be discussed ahead.

The boundary size for a transition between cohesive and non-cohesive powders is not precisely defined in the literature, but it is agreed that the intensity of van der Waals forces is enhanced by the presence of particles of sizes less than 100 μm, owing to the increase in the specific superficial area and in the number of contacts between particles per unit of volume (Castellanos, 2005). To investigate the possible reasons for the poor flowability of powder C, its particle size distribution was measured using a laser diffraction technique, in Malvern Mastersizer (MAF5001). Triplicate measurements were performed and the data revealed that 14% of the volume fraction in this sample was composed of particles with sizes less than 100

μm. In spite of the small volume fraction, these fines correspond to about 93% of the specific superficial area in this sample. Therefore, the tendency towards a cohesive behavior of sample C is justified by the presence of these fine particles which were not detected in the sieving analysis, possibly because they agglomerate and are retained in the sieve with an aperture of 150 μm. Although the presence of fines is noticed in all the samples in the micrographs from Figure 1, the amount is greater in sample C and the impact of fines on powder cohesiveness is more significant in this sample owing to the substantial increase in the specific superficial area. The presence of agglomerates in sample C is corroborated by its high void fraction, as seen in Table 1.

The data in Fig. 2 shows that HR of the mixtures initially decreases steeply at a practically linear rate in the range of d_s from 225 to 550 μm, and tend to a constant value close to 1.25 for particle sizes over 400 μm. An exponential equation, represented by the solid line in Fig. 2, was fitted to the experimental data, with a correlation coefficient R^2=0.90. The equation is given by:

$$HR = 1 + e^{-0.003 d_S} \tag{7}$$

The uniform distribution of the data around the fitting line in Fig. 2 suggests no evidence of an influence of the particle size distribution in HR.

The results for AoR are shown in Fig. 3. The wider dispersion in AoR measurements in comparison to HR can be attributed to the uncertainties that arise from the loose consolidation state of the conical heap formed in the AoR measurements, as the random arrangement of particles is hardly reproducible in different assays in spite of the attempts to standardize the experimental procedures. This problem is minimized in the HR measurements, as the initially loose-packed bed goes towards a quasi-consolidated state throughout tapping.

(Fig. 3)

In spite of the wide dispersion, the data show a consistent decrease in AoR as the particle size increases. Like the results for HR, the values of AoR for powders A and B are quite similar (respectively 42±1° and 42.3±0.8^{o}) and indicative of a *passable* flowability. It increased up to 46.7±0.3^{o} for powder C, characterizing a *very poor* flowability for this sample. The results for the powder mixtures are intermediate between powders A (the coarsest) and C (the finest). A polynomial equation was fitted to experimental data (represented by the solid line in Fig. 3), however, in view of the wide dispersion of data, the correlation coefficient was too low (R^2=0.43). The equation is given by:

$$AoR = 91.99 d_S^{-0.122} \quad (8)$$

As suggested by some authors (Geldart, Abdullah, Hassanpour, Nwoke, & Wouters, 2006; Wouters & Geldart, 1996), the correlation could be improved by using the weighted AoR (defined as the ratio of AoR to the loose bulk density) to replace AoR.

It is worth noting in Fig. 3 that, even at similar mean particle sizes, the AoR of the binary mixtures made of A and C powders are always significantly higher than the ones measured for the mixtures of B and C, suggesting that the angle is sensitive to the relative size of powders in the mixture and also to particle size distribution.

The transition from a *passable* to a *poor* flowability (AoR>45°) is observed for a particle size close to 350 μm, which agrees with the results observed for HR. This result confirms that both indexes are good indicators of powder flowability and yields to consistent predictions, despite the mean size obtained from sieving is not representative of powders' PSD.

A comparison of HR and AoR of powders A and B to those of other biomasses with similar mean sizes (Lam & Sokhansanj, 2014) shows that SCG flowability indexes obtained in the present study are close to those reported for switchgrass, which is an ease flow biomass. It is worth noting that the flowability indexes of SCG were more sensitive to the variation of particle mean size than other regular biomasses. A decrease in d_s from 550 to 225 μm increased HR and AoR indexes of SCG by approximately 19.3 and 13.7%, respectively, while a similar variation increased HR and AoR of switchgrass, corn stover and wheat straw in only 5%.

The correlation between the weighted AoR and HR can be observed in Fig. 4. The experimental data fitted an exponential equation with R^2=0.92. The equation is given by:

$$AoR/\rho_{lb} = 0.017e^{1.54HR} \quad (9)$$

The detail in Fig. 4 shows the data of the pure AoR as a function of HR, which clearly yields a significantly poorer fitting.

(Fig. 4)

As aforementioned, the AC binary mixtures (with coarser particles and wider size span), always presented worse flowability in comparison to the BC mixtures, which is evidence of the influence of the particle size distribution (PSD) on AoR. We observed that the loose bulk densities of AC mixtures were on average 5% higher than those of BC mixtures, which contributes to form taller heaps with higher AoR in AC mixtures.

Presenting the flowability of powders as a function of the mean diameter is a useful and common practice. However, this approach may lead to misleading conclusions as powders with different PSD and similar mean diameter can present distinct flow behavior. This is the case, for example, of the base powder B (d_S=400 μm, AoR=42.3° and HR=1.21) and the

ternary mixture $A_{60\%}B_{20\%}C_{20\%}$ (d_S=403 μm, AoR=45.4° and HR=1.30). Based on these values, the flowability of the first powder is classified as *passable* and the second's as *poor*.

In the next section, the validity of the Modified Linear-Packing model (Yu & Standish, 1991) to predict the loose and tapped packed-bed void fractions for the powder mixtures is evaluated.

3.4 Modified Linear-Packing model to predict ε_b of the SCGs mixtures

According to Figures 2 and 3, the flowability indexes of the binary and ternary mixtures are in between the values obtained for the largest (A) to the finest (C) powders. Therefore, the Modified Linear-Packing model (Yu, Bridgwater, & Burbidge, 1997) was applied to predict the void fraction of packed-beds of variable composition. The small-to-large ratios of the mixtures (R_{ij}) were calculated from the mean sizes of A, B and C ($d_{SA}>d_{SB}>d_{SC}$), and yielded the values R_{BA}=0.73, R_{CB}=0.56, and R_{CA}=0.41. The interaction functions $f(R_{ij})$ and $g(R_{ij})$, that depend only on R_{ij}, were determined by Eqs. (10) and (11), recommended for spherical and non-spherical particles (Yu, Zou, & Standish, 1996).

$$f(R_{ij}) = (1 - R_{ij})^{3.33} + 2.81.R_{ij}.(1 - R_{ij})^{2.77} \quad (10)$$

$$g(R_{ij}) = (1 - R_{ij})^{1.97} + 0.36.R_{ij}.(1 - R_{ij})^{3.67} \quad (11)$$

The bed void fraction (ε) was then calculated by Eq. (12), in which V is the specific volume of the powder mixture. In this study, the mixtures were produced by combining the three base powders, therefore variable V was obtained from Eqs. (13) to (16). The values of V_A, V_B, and V_C were calculated from Eq. (12) using the experimental values of loose or tapped void fractions (Table 1), according to the packing state to be determined.

$$\varepsilon = (V - 1)/V \tag{12}$$

$$V = \max\{V_A^T, V_B^T, V_C^T\} \tag{13}$$

$$V_A^T = V_A . y_A + V_B . \left(1 - f(R_{BA})\right) . y_B + V_C . [1 - f(R_{CA})] . y_c \tag{14}$$

$$V_B^T = [V_A - (V_A - 1) . g(R_{BA})] . y_A + V_B . y_B + V_C . [1 - f(R_{CB})] . y_C \tag{15}$$

$$V_C^T = [V_A - (V_A - 1) . g(R_{CA})] . y_A + [V_B - (V_B - 1) . g(R_{CB})] . y_B + V_C . y_C \tag{16}$$

As shown in Fig. 5, the experimental void fractions are quite well predicted by the model, for both loose and tapped conditions, with mean deviations less than 2%. The experimental values of void fractions were estimated by Eq. 2 as the base samples present low moisture content, as shown in Table 1.

(Fig. 5)

The loose and tapped predicted void fractions were used in Eq. (2) to calculate the bulk densities of powders and HR was obtained for the binary and ternary mixtures. The predicted (solid lines) and measured (symbols) values of HR are presented in Fig. 6 as a ternary diagram, where each vertex corresponds to a pure base sample (A, B or C), the edges correspond to the binary mixtures (AB, AC, and BC) with a variable mass fraction from 0 to 100%, and the interior corresponds to the ternary mixtures (ABC). For example, the point marked with the star symbol on side line A-C of Fig. 6 shows that HR of a binary mixture composed of 60% of A and 40% of C is equal to 1.33. For a ternary mixture with 60% of A, 20% of B and 20% of C (the star symbol inside the triangle), the value of HR is 1.26. According to (Yu & Standish, 1991), when the ratio between particle sizes is higher than 0.154, as is the case of our mixtures, powder compaction occurs mainly by the occupation mechanism, in which the voids are filled in throughout packing as the smaller particles occupy the spaces opened by particle rearrangement. In a packing ruled by such a mechanism, all the components in the mixture contribute to the compaction kinetic. In spite of that, HR of

the SCG mixtures was affected mostly by the mass fraction of the finer particles (powder C), as the smaller and more cohesive particles limit the packed-bed structure rearrangement in order to achieve a closer packing (Lam & Sokhansanj, 2014).

(Fig. 6)

Based on HR results shown in Fig. 6, it can be seen that powder flowability worsen as the mass fraction of powder C is raised. Therefore, powders with y_c=0 have flowability categorized as *fair*; with y_c=0.2 the flowability is *passable*; in the interval 0.4≤ y_c≤ 0.6 it is *poor* and with y_c≥0.8 it is *very poor*. For y_c>0.5 the HR increases linearly with the increase in y_c, indicating that powder flowability is governed by the finest particles and the presence of coarse particles did not alter the flowability. As AoR is directly correlated to HR, as shown in Fig. 4 (or Eq. 9), the increase in the amount of powder C in a mixture also increases AoR.

It is worth noting that the ternary diagram proposed in Fig. 6 can be used to predict the HR for a sample sieved and cut into three fractions with mean sizes similar to the base samples A, B and C. New diagrams would need to be made for fractions with different sizes. Nevertheless, using a ternary diagram as a graphical representation of changes in HR could be a useful tool for a rapid and reliable estimation of HR and the method can be extended for other powders.

In the next section, the flowability indexes of SCG will be evaluated for moistures up to approximately 50% w.b., which cover the usual processing range (Silva et al., 1998).

3.6 Effect of moisture content on the flowability indexes

The values of HR and AoR data for powders under different moisture contents are presented in Table 2.

(Table 2)

As the moisture content of the base samples was raised up to 50% w.b., HR stays practically constant and AoR shows a discrete increase, although in most conditions the difference is within the range of experimental uncertainty. It is known from the literature that increasing moisture content is likely to affect the powder flow behavior and mechanical strength as the packing reaches the funicular state, at saturation levels between 25% and 50%, when saturated clusters and liquid bridges coexist (Althaus & Windhab, 2012). In the range of conditions tested, a slight deterioration in flowability was observed for powder C only at a saturation level close to 42%, corresponding to a moisture content of 59.2%. This indicates that the bridging forces were strong enough to significantly affect the flowability index in this condition. Therefore, for S<42% the samples may be in the pendular state, in which liquid bridges exist but do not play a significant role on the flow behavior. It is worth noting that the value of S=42% found in this study is between 25% and 50%, which is reported as a transition range from the pendular to the funicular states for real systems (Althaus & Windhab, 2012).

Since the dried and moist base samples presented similar HR up to 50% w.b., the diagram presented in Fig. 6 can be used for moist powders up to this range.

Based on the analysis of the previous sections, some alternatives to estimate HR and AoR of non-consolidated SCG powders are suggested:

- The Eq. (7), valid in the range 225<ds<550 µm can be used to estimate HR if the powder mean diameter is known. In addition, by measuring powder loose bulk density, Eq. (9) can provide estimates for AoR.
- If the powder size can be expressed as a composite of three mass fractions of different sizes, the ternary diagram presented in Fig. 6 can be used to estimate HR and AoR can be estimated from Eq. (9).

- Inversely, Eq. (9) can be used to obtain HR if powder AoR and loose bulk density are measured. Based on the measured values of HR, the ternary diagram can be used as a tool to evaluate the mass fraction of each base sample in the binary or ternary mixtures.

These procedures are based on quick and easy measurements and may be useful to help in process design and monitoring unit operations involved in renewable energy generation in soluble coffee facilities.

4. Conclusions

This study presented experimental data of HR and AoR of non-consolidated SCG powder mixtures prepared from combinations of three base samples and with mean sizes from 225 to 550 μm. The measured indexes showed that a *poor* flowability is observed for SCG powders with d_S <350 μm or for mixtures with a fraction greater than 40% in mass of fines. The AoR of SCG mixtures was influenced by the PSD, as samples with wider size span presented higher AoR. The HR of the mixtures increased significantly as the amount of the finest and more cohesive sample rose. The flowability behavior of moist SCGs was similar to that of dried powders for moisture contents up to 50% (w.b.). It was verified that SCGs present a higher energy density and worse flowability indexes when compared to other ordinary biomasses. Finally, some procedures to identify flowability indexes based on fitted correlations and on the Linear Mixture-Packing Model were proposed. These procedures may be useful to improve handling and monitoring operations in plants that use SCGs for thermochemical applications.

Acknowledgements

The authors would like to thank the São Paulo Research Foundation (FAPESP), grant 2016/25946-2, for the financial support.

Nomenclature

AoR	Angle of repose, defined by Eq. (6) (°)
D	Mean diameter of the circumference of the conical powder bed (cm)
d	Diameter of the funnel discharge orifice (cm)
d_s	Mean diameter, defined by Eq. 1 (µm)
d_{svi}	Mean sieve diameter of a base sample, i = A, B or C (µm)
$f(R_{ij})$	Interaction function defined by Eq. (10) (-)
$g(R_{ij})$	Interaction function defined by Eq. (11) (-)
H	Height of the conical bed (cm)
HR	Hausner ratio, defined by Eq. (5) (-)
MC	Moisture content (%)
N	Number of taps (-)
p	Significance level (-)
R_{ij}	Ratio of small (i) to large (j) mean diameter (-)
S	Water saturation level, defined by Eq. (4) (-)
y_i	Mass fraction of a base sample in the mixture, i = A, B or C (-)
V	Specific volume, defined by Eq. (13) (-)
V_i	Specific volume of a base sample, i = A, B or C, determined by Eq. (12). (-)
V_i^T	Specific volume for i = A, B or C, defined by Eqs. (14) to (16)
V_s	Volume occupied by solids in the packed-bed (m^3)
V_t	Total volume of the dry tapped packed-bed (m^3)
V_w	Total volume of liquid water in the packed-bed (m^3)

Greek letters

ε	Void fraction, defined by Eq. (2) (-)
ε_{lb}	Void fraction for loose bulk condition (-)
ε_{tb}	Void fraction for tapped bulk condition (-)

ρ_{lb}	Loose bulk density for N=0 (kg/m³)
ρ_p	Particle density (kg/m³)
ρ_s	Solid density (kg/m³)
ρ_{tb}	Tapped bulk density for N=1250 (kg/m³)

References

Abdullah, E., & Geldart, D. (1999). The use of bulk density measurments as a flowability indicators. *Powder Technology*, *102*, 151–165. https://doi.org/10.1017/CBO9781107415324.004

Al-Hamamre, Z., Foerster, S., Hartmann, F., Kröger, M., & Kaltschmitt, M. (2012). Oil extracted from spent coffee grounds as a renewable source for fatty acid methyl ester manufacturing. *Fuel*, *96*, 70–76. https://doi.org/10.1016/j.fuel.2012.01.023

Althaus, T. O., & Windhab, E. J. (2012). Characterization of wet powder flowability by shear cell measurements and compaction curves. *Powder Technology*, *215–216*, 59–65. https://doi.org/10.1016/j.powtec.2011.09.007

ASTM International. (2000). Standard test method for measuring the angle of repose of free-flowing mold powders. *ASTM C1444-00*, (1), 15–16. https://doi.org/10.1520/C1444-00

ASTM International. (2010). Standard test method for sieve analysis of fine and coarse aggregates. *ASTM C136-01*, 1–5. https://doi.org/10.1520/C0136-06.2

Ballesteros, L. F., Teixeira, J. A., & Mussatto, S. I. (2014). Chemical, functional, and structural properties of spent coffee grounds and coffee silverskin. *Food and Bioprocess Technology*, *7*(12), 3493–3503. https://doi.org/10.1007/s11947-014-1349-z

Brazilian Coffee Exporters Council. (2017). Monthly coffee report. Retrieved March 2, 2018, from http://www.cecafe.com.br/en/publications/monthly-exports-report/

Campos-Vega, R., Loarca-Piña, G., Vergara-Castañeda, H. A., & Oomah, B. D. (2015). Spent coffee grounds: a review on current research and future prospects. *Trends in Food Science & Technology*, *45*, 24–36. https://doi.org/10.1016/j.tifs.2015.04.012

Campos, M. M., & Ferreira, M. C. (2013). A comparative analysis of the flow properties between two alumina-based dry powders. *Advances in Materials Science and Engineering*, *2013*(519846), 1–7. https://doi.org/10.1155/2013/519846

Castellanos, A. (2005). The relationship between attractive interparticle forces and bulk behaviour in dry and uncharged fine powders. *Advances in Physics*, *54*(4), 263–376. https://doi.org/10.1080/17461390500402657

Dai, J., Cui, H., & Grace, J. R. (2012). Biomass feeding for thermochemical reactors. *Progress in Energy and Combustion Science*, *38*, 716–736. https://doi.org/10.1016/j.pecs.2012.04.002

Dhiman, J., Shrestha, A., Fasina, O., Adhikari, S., Via, B., & Gallagher, T. (2016). Physical, ignition, and volatilization properties of biomass feedstocks dusts. *Transactions of the ASABE*, *58*(6), 1425–1437. https://doi.org/10.13031/trans.58.11233

Geldart, D. (1973). Types of gas fluidization. *Powder Technology*, *7*(5), 285–292. https://doi.org/10.1016/0032-5910(73)80037-3

Geldart, D., Abdullah, E. C., Hassanpour, A., Nwoke, L. C., & Wouters, I. (2006). Characterization of powder flowability using measurement of angle of repose. *China Particuology*, *4*(3–4), 104–107. https://doi.org/10.1016/S1672-2515(07)60247-4

Guo, Z., Chen, X., Xu, Y., & Liu, H. (2015). Study of flow characteristics of biomass and biomass-coal blends. *Fuel*, *141*, 207–213. https://doi.org/10.1016/j.fuel.2014.10.062

Instant Coffee Market. (2017). Instant coffee market: global industry trends, share, size, growth, opportunity and forecast 2017-2022. Retrieved March 2, 2018, from http://www.imarcgroup.com/instant-coffee-processing-plant

International Coffee Organization. (2017). Total coffee production by all exporting countries. Retrieved March 2, 2018, from http://www.ico.org/prices/po-production.pdf

Kondamudi, N., Mohapatra, S. K., & Misra, M. (2008). Spent coffee grounds as a versatile source of green energy. *Journal of Agricultural and Food Chemistry*, *56*, 11757–11760. https://doi.org/10.1021/jf802487s

Lam, P. S., & Sokhansanj, S. (2014). Engineering properties of biomass. In Y. Shastri, A. Hansen, L. Rodríguez, & K. C. Ting (Eds.), *Engineering and Science of Biomass Feedstock Production and Provision* (1st ed., Vol. 1, pp. 17–35). New York: Springer New York. https://doi.org/10.1007/978-1-4899-8014-4

Li, P., Kanda, H., & Makino, H. (2014). Simultaneous production of bio-solid fuel and bio-crude from vegetal biomass using liquefied dimethyl ether. *Fuel*, *116*, 370–376. https://doi.org/10.1016/j.fuel.2013.08.020

Li, Q., Rudolph, V., Weigl, B., & Earl, A. (2004). Interparticle van der Waals force in powder flowability and compactibility. *International Journal of Pharmaceutics*, *280*, 77–93. https://doi.org/10.1016/j.ijpharm.2004.05.001

Liu, Y., Tu, Q., Knothe, G., & Lu, M. (2017). Direct transesterification of spent coffee grounds for biodiesel production. *Fuel*, *199*, 157–161. https://doi.org/10.1016/j.fuel.2017.02.094

Mallol, G., Amorós, J. L., Orts, M. J., & Llorens, D. (2008). Densification of monomodal quartz particle beds by tapping. *Chemical Engineering Science*, *63*, 5447–5456. https://doi.org/10.1016/j.ces.2008.07.032

Mussatto, S. I., Machado, E. M. S., Martins, S., & Teixeira, J. A. (2011). Production, composition, and application of coffee and its industrial residues. *Food and Bioprocess Technology*, *4*, 661–672. https://doi.org/10.1007/s11947-011-0565-z

Organization, W. H. (2012). Bulk density and tapped density of powders. *QAS/11.450 - The International Pharmacopeia*, 1–6. https://doi.org/10.1007/s13398-014-0173-7.2

Silva, M. A., Nebra, S. A., Machado Silva, M. J., & Sanchez, C. G. (1998). The use of biomass residues in the brazilian soluble coffee industry. *Biomass and Bioenergy*, *14*(5–6), 457–467. https://doi.org/10.1016/S0961-9534(97)10034-4

Singh, P. C., Singh, R. K., Bhamidipati, S., Singh, S. N., & Barone, P. (1997). Thermophysical properties of fresh and roasted coffee powders. *Journal of Food Process Engineering*, *20*(1), 31–50. https://doi.org/10.1111/j.1745-4530.1997.tb00409.x

Tan, G., Morton, D. A. V., & Larson, I. (2015). On the methods to measure powder flow. *Current Pharmaceutical Design*, *21*(40), 5751–5765. https://doi.org/10.2174/1381612821666151008125852

Wouters, I. M. F., & Geldart, D. (1996). Characterising semi-cohesive powders using angle of repose. *Particle & Particle Systems Characterization*, *13*, 254–259.

Yu, A. B., Bridgwater, J., & Burbidge, A. (1997). On the modelling of the packing of fine particles. *Powder Technology*, *92*(3), 185–194. https://doi.org/10.1016/S0032-5910(97)03219-1

Yu, A. B., & Standish, N. (1991). Estimation of the porosity of particle mixtures by a linear-mixture packing model. *Industrial and Engineering Chemistry Research*, *30*(6), 1372–1385. https://doi.org/10.1021/ie00054a045

Yu, A. B., Zou, R. P., & Standish, N. (1996). Modifying of the linear packing model for predicting the porosity of nonspherical particle mixtures. *Industrial & Engineering Chemistry Research*, *35*(10), 3730–3741. https://doi.org/10.1021/ie950616a

Zarrinbakhsh, N., Wang, T., Rodriguez-Uribe, A., Misra, M., & Mohanty, A. K. (2016). Characterization of wastes and coproducts from the coffee industry for composite material production. *BioResources*, *11*(3), 7637–7653. https://doi.org/10.15376/biores.11.3.7637-7653

Figure 1

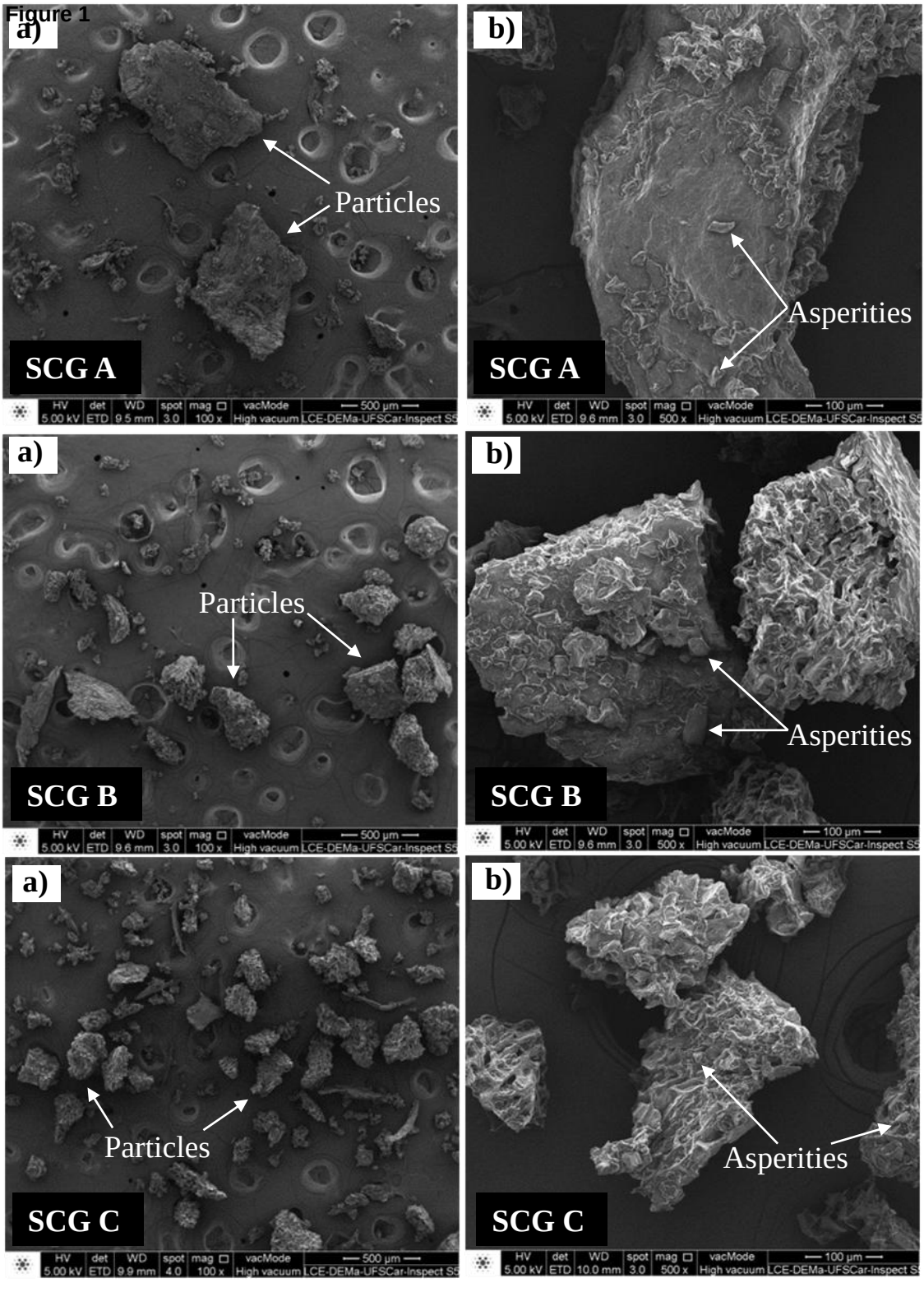

Fig. 1. Micrographs of A, B and C samples. (a) 100x and (b) 500x magnification.

Figure 2

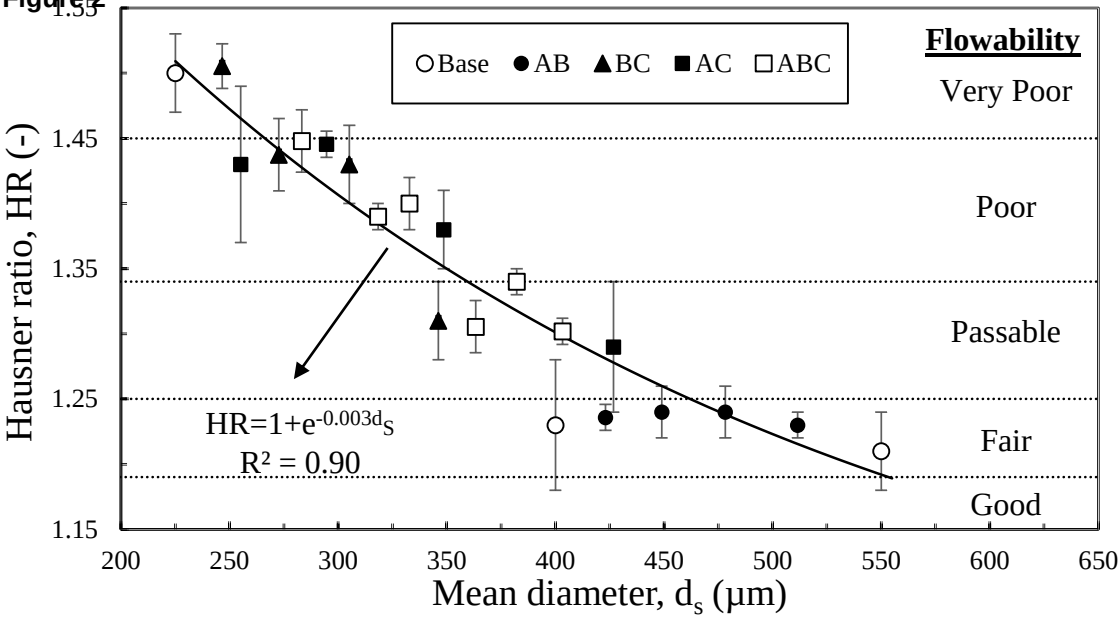

Fig. 2. Hausner ratio as a function of mean diameter for the base samples, binary (AB, AC, and BC) and ternary mixtures (ABC) of SCG powders.

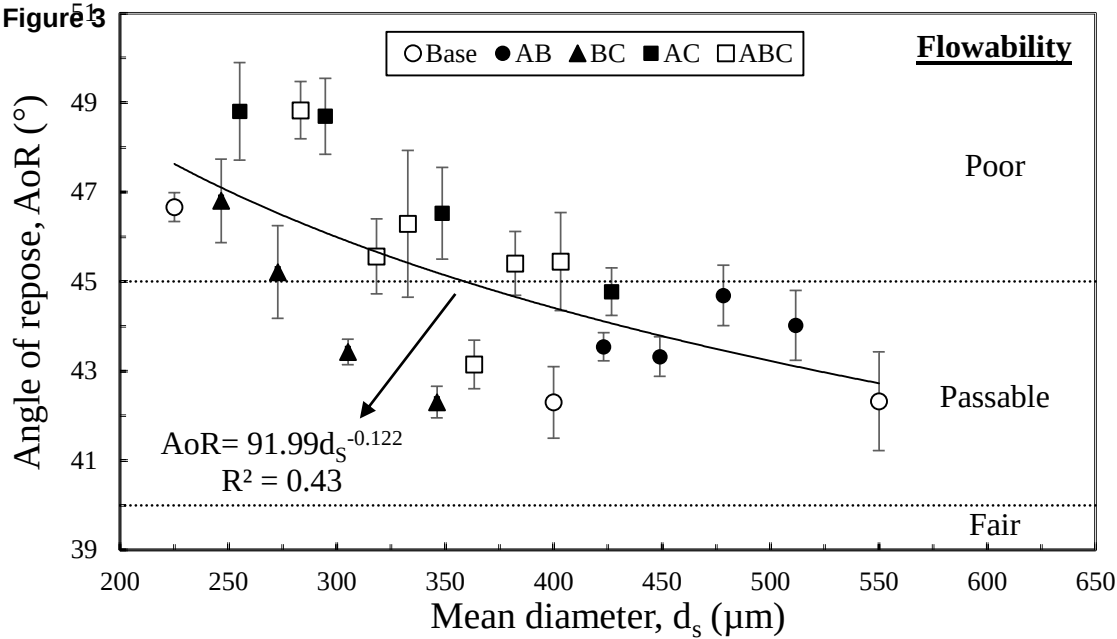

Fig. 3. Repose angle as a function of mean diameter for the base samples, binary (AB, AC, and BC) and ternary mixtures (ABC) of SCG.

Figure 4

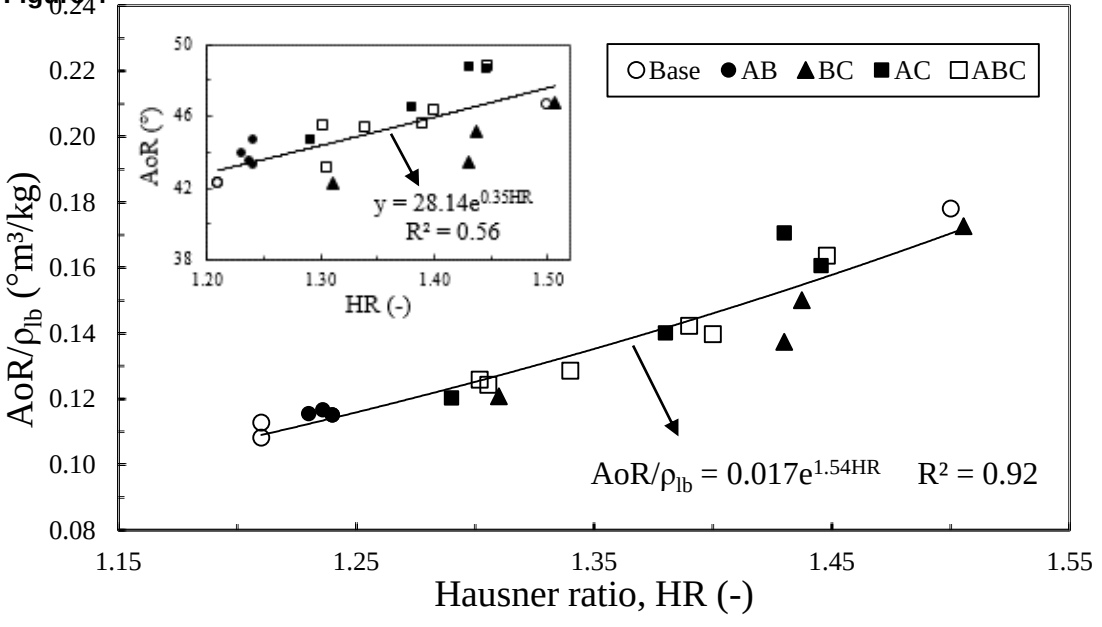

Fig. 4. Weighted AoR versus HR for SCG powders.

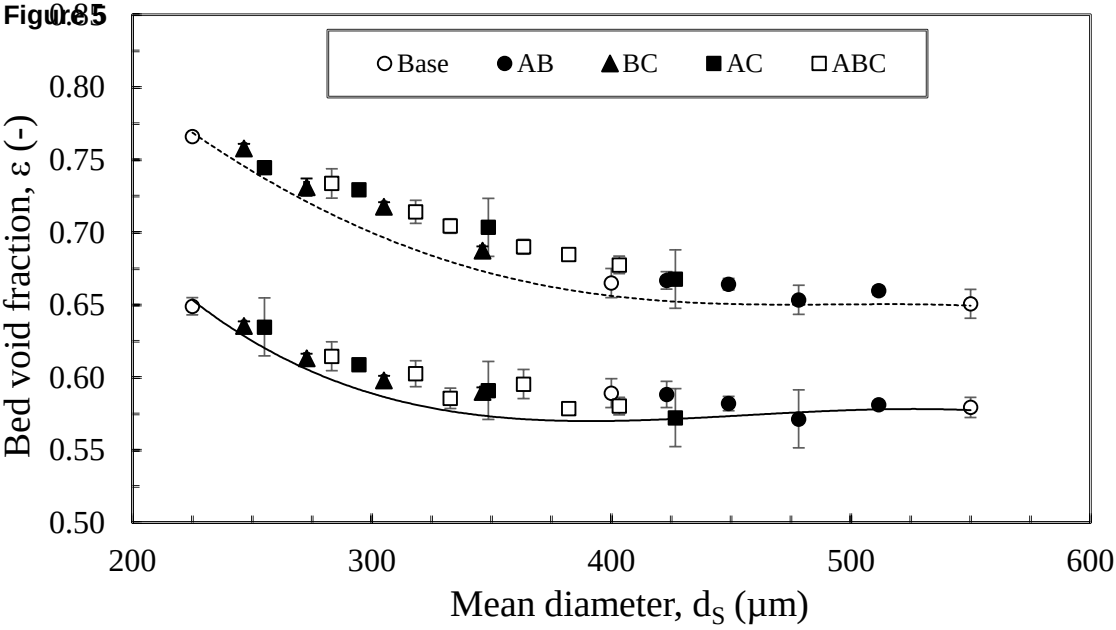

Fig. 5. Porosities as a function of mean diameter for the SCG base samples, binary and ternary mixtures: —, tapped and ---, loose porosities predicted by the Modified Linear-Packing model.

Figure 6

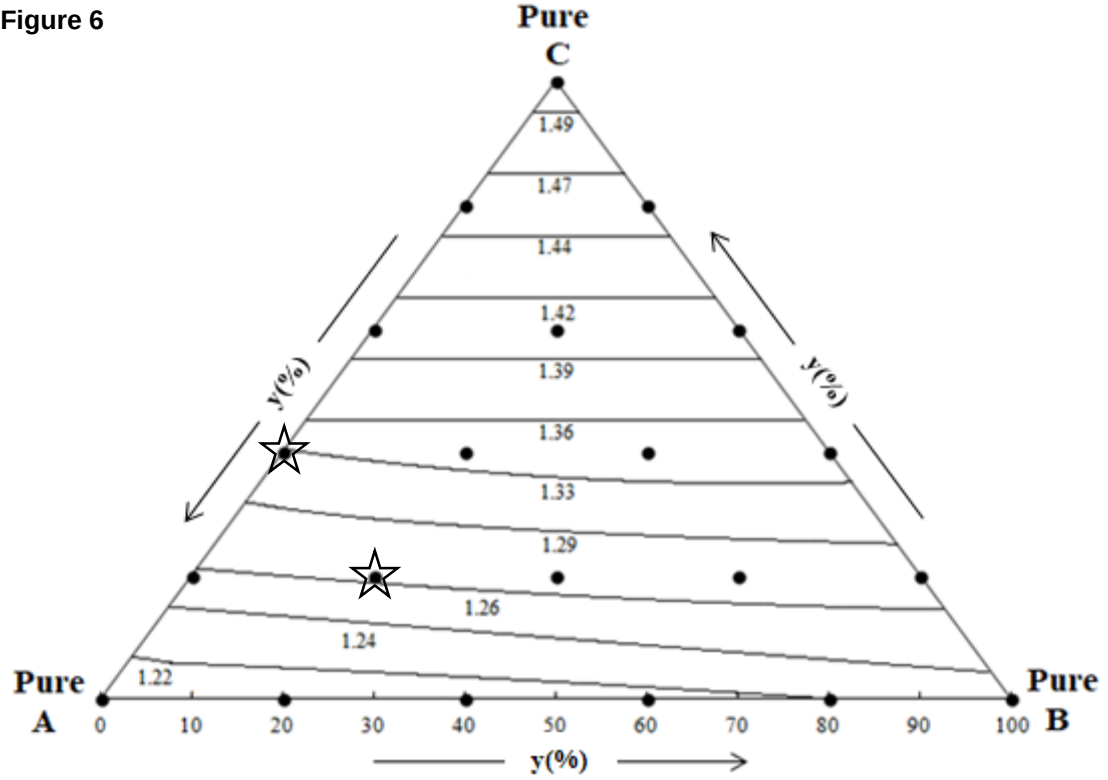

Fig. 6. HR values for SCG powders as a function of base samples composition (y): ●, HR measured points; —, predicted by the Modified Linear-Packing model.

Table 1

Table 1. Sieve mean diameter, moisture content, particle density, loose and tapped bulk densities and porosities for the base powders.

SCG Powder	d_{sv} (µm)	Moisture content (% w.b.)	ρ_p (kg/m³)	ρ_{lb} (kg/m³)	ρ_{tb} (kg/m³)	ε_{lb} (-)	ε_{tb} (-)
A	550	5.4 ± 0.1[a]	1130 ± 10[a]	390 ± 20[a]	471 ± 7[a]	0.655 ± 0.010[a]	0.583 ± 0.009[a]
B	400	2.8 ± 0.1[b]	1120 ± 20[a]	380 ± 20[a]	460 ± 10[a]	0.660 ± 0.010[a]	0.590 ± 0.010[a]
C	225	3.2 ± 0.1[c]	1120 ± 10[a]	262 ± 2[b]	393 ± 7[b]	0.766 ± 0.001[b]	0.649 ± 0.006[b]

Values with different letters in the same column are significantly different at a 0.05 significance level.

Table 2

Table 2. Flowability of the base samples as a function of moisture content and water saturation level.

SCG Sample	MC (% w.b.)	S (%)	HR (-)	AoR (º)
	5.4 ± 0.1	3.8 ± 0.1	1.21 ± 0.03[ab]	42.0 ± 1.0[ab]
	21.1 ± 0.5	13.3 ± 0.3	1.19 ± 0.01[ab]	43.0 ± 1.0[ab]
A	30.4 ± 0.2	17.3 ± 0.1	1.17 ± 0.01[ab]	43.2 ± 0.7[ab]
	37.9 ± 0.1	20.8 ± 0.1	1.17 ± 0.01[a]	43.2 ± 0.6[ab]
	47.0 ± 1.0	27.3 ± 1.0	1.21 ± 0.02[b]	44.1 ± 0.4[b]
	2.8 ± 0.1	2.1 ± 0.1	1.21 ± 0.05[a]	42.3 ± 0.8[a]
	19.4 ± 0.9	12.5 ± 0.3	1.23 ± 0.02[a]	45.8 ± 0.2[b]
B	28.6 ± 0.7	16.1 ± 0.5	1.21 ± 0.01[a]	45.0 ± 1.0[b]
	36.8 ± 0.9	20.0 ± 0.8	1.25 ± 0.02[a]	44.8 ± 0.8[b]
	44.5 ± 0.5	26.3 ± 0.3	1.30 ± 0.07[a]	46.1 ± 0.5[b]
	3.2 ± 0.1	1.8 ± 0.1	1.50 ± 0.03[ab]	46.7 ± 0.3[a]
	29.6 ± 0.3	14.5 ± 0.4	1.45 ± 0.04[ab]	48.7 ± 0.9[b]
C	42.0 ± 0.1	21.6 ± 0.2	1.44 ± 0.02[a]	50.9 ± 0.2[c]
	52.4 ± 0.4	31.1 ± 0.6	1.53 ± 0.02[b]	52.0 ± 0.5[c]
	59.2 ± 0.1	42.0 ± 0.2	1.62 ± 0.05[c]	54.9 ± 0.3[d]

Values with different letters in the same column are significantly different at a 0.05 significance level.